Applied Catalysis B: Environmental 230 (2018) 29–35

Contents lists available at ScienceDirect

Applied Catalysis B: Environmental

journal homepage: www.elsevier.com/locate/apcatb

In search of membrane-catalyst materials for oxidative coupling of methane: Performance and phase stability studies of gadolinium-doped barium cerate and the impact of Zr doping

Valentina Omoze Igenegbai[a], Randall J. Meyer[b], Suljo Linic[a,*]

[a] Department of Chemical Engineering, University of Michigan, Ann Arbor, MI, USA
[b] Corporate Strategic Research, ExxonMobil Research and Engineering, Annandale NJ USA

ARTICLE INFO

Keywords:
Oxidative methane coupling
Solid oxide membrane-catalyst
Gadolinium-doped barium cerate
Catalyst performance
Phase stability

ABSTRACT

Oxidative coupling of methane (OCM) is a promising technology for the direct conversion of methane to ethylene and ethane (C_2). This process is yet to be commercialized due its poor yield reflected in the formation of undesired products such as CO and CO_2 (CO_x) as methane conversion increases, particularly in conventional packed bed reactors (PBRs). It has been argued that by applying O^{2-} conducting membrane reactors that distribute the oxygen feed, the selectivity to the C_2 products can be increased. A practical design for these membrane reactors would include combining a selective catalyst, preferably O^{2-} conducting, with an O^{2-} conducting membrane. In this work, we studied an O^{2-} conducting material, gadolinium-doped barium cerate ($BaCe_{0.8}Gd_{0.2}O_{3-\delta}$ or BCG), to evaluate its potential applicability as a catalyst and membrane in OCM membrane reactors. From PBR tests, we found that this material was active for OCM, and achieved a maximum C_{2+} yield of ~14% at 1023 K. Furthermore, at low oxygen partial pressures, a C_{2+} selectivity of ~90% was obtained at methane conversions of ~3%. Although the C_{2+} yield from this material was stable over 48 h on stream at high methane conversions, X-ray diffraction data showed that the BCG perovskite phase, which is required for its conductive (membrane) properties, decomposes into $BaCO_3$, CeO_2 and Gd_2O_3 like phases, due to reactions with CO_2. We showed that doping BCG with Zr was effective at suppressing the phase instability in OCM without significantly affecting the C_{2+} yields.

1. Introduction

Natural gas is an abundant resource with over 300 trillion cubic feet of proven reserves [1]. Its production is projected to increase due to the availability of unconventional sources such as shale gas, and the possibility of harnessing methane hydrates in the long term [2,3]. It is composed mainly of methane which has vast potential as an advantaged feedstock for chemical and fuel production. In general, converting methane directly into chemicals under mild conditions is challenging due to its strong C—H bonds (bond strength ~434 kJ/mol) [3–5]. Commercially, methane is converted through a high temperature, energy intensive reforming process to syngas (mixture of mainly CO and H_2), which is then used to produce chemicals such as methanol and higher hydrocarbons. This indirect conversion of methane to chemicals via syngas production is only commercially practical when applied on a large scale. Consequently, methane from isolated small-scale sources (e.g., associated gas), that cannot be economically transported, is commonly flared causing the release of greenhouse gases [3,5]. Direct conversion of methane into valuable chemicals can alleviate the need for costly syngas production and is potentially more suitable for valorizing methane released from small scale sources. Therefore, there is significant interest in the development of direct methane conversion routes [5–7].

A potential route for direct methane conversion is through a process known as the oxidative coupling of methane (OCM) which was first reported in the early 1980s [8]. In OCM, methane is activated at high temperatures (923–1173 K) in the presence of oxygen and an active catalyst to produce C_2 hydrocarbons (ethane and ethylene) [9]. It has been proposed that during OCM, hydrogen is abstracted from methane to form methyl radicals which couple in the gas phase to form ethane [6,10,11]. The ethane formed is subsequently dehydrogenated to ethylene through catalytic and gas phase reaction steps [7,12]. Various mixed metal oxide catalysts have been investigated for OCM and some of the best C_2 yields have been achieved on $Mn/Na_2WO_4/SiO_2$ and Li/MgO catalysts [13,14]. Even for these catalysts, the reported performance have largely remained below the widely-cited commercial

* Corresponding author.
E-mail address: linic@umich.edu (S. Linic).

https://doi.org/10.1016/j.apcatb.2018.02.040
Received 5 November 2017; Received in revised form 16 February 2018; Accepted 17 February 2018
Available online 19 February 2018
0926-3373/

viability target of a minimum single-pass C_2 yield of ~30% at a C_2 selectivity of ~90%, using undiluted feed streams [15,16].

A fundamental issue with OCM is that, at the high temperatures applied, undesired over oxidation products such as CO and CO_2 (CO_x) are more thermodynamically favored than the C_2 products [15]. Furthermore, when conventional co-fed packed bed reactors (PBRs) are used, the desired C_2 products can be converted sequentially to CO_x at relatively higher rates [12,17], and in general the C_2 selectivity decreases as methane conversion increases. It has also been demonstrated that the C_2 selectivity in OCM is higher at lower oxygen partial pressures (i.e. higher CH_4/O_2 ratios) [12,18]. These observations have been used to argue that reactors with a distributed oxygen feed, such as a membrane reactor, can give significantly higher C_2 yields than a packed bed plug flow reactor modeled under the same operating conditions [15].

The most common type of membrane reactor studied in OCM are solid oxide membranes which operate at high temperatures (> 923 K). The configuration of these membranes is such that the methane and oxygen-containing streams (e.g., air) are separated by an ion-conducting membrane which transfers O^{2-} from the oxygen side to the methane side where the OCM reaction occurs. An added advantage of this membrane reactor is that it is able to supply the catalyst with pure oxygen from air without a costly separation step due to the lack of transfer of other air components (e.g., N_2) [15]. For these membranes to conduct O^{2-} effectively, there is a need for countercurrent flow of electrons to fulfill overall charge neutrality in the membrane. This is commonly achieved by using a mixed ionic and electronic conducting (MIEC) membrane, where the electrons are transferred through the membrane itself in the opposite direction of O^{2-}

Several experimental studies have shown that when solid oxide membrane reactors are compared to packed bed reactors co-fed with both the methane and oxygen-containing stream, higher C_2 selectivity can be achieved in the former [19–23]. However, the performance of these membrane systems in OCM are also generally below the techno-economic target [15,24]. An issue that has limited the performance of membrane reactors in OCM is the relatively low oxygen fluxes through the membranes which, aside from limiting methane conversion, promotes carbon deposition and catalyst/membrane deactivation. In general, MIEC membranes doped with transition metal ions (e.g., Co and Fe) give higher oxygen fluxes [25]. However, it has been demonstrated that the presence of transition metal ions in membrane materials leads to a dramatic decline in OCM selectivity [26].

In the present study, we aim to develop alternative O^{2-} conducting materials that are selective for OCM. This step is considered crucial to the advancement of OCM membrane reactors. Specifically, we focus our attention on doped barium cerates because they are a class of high temperature O^{2-} conducting membrane materials composed of elements that have been shown to be selective in OCM [9,21,27–29]. A critical problem in using doped barium cerate membranes in OCM is that the perovskite structure of barium cerate ($BaCeO_3$) is prone to destruction on prolonged exposure to CO_2-containing atmospheres [30]. This phase instability has been attributed to a thermodynamically favorable reaction of the perovskite with CO_2 to form $BaCO_3$ and CeO_2 at temperatures below ~1373 K [30–32]. Destruction of the perovskite structure can lead to conductivity losses and mechanical failure which are both detrimental to the performance of these membrane reactors [33].

In this contribution, we study the performance and stability of gadolinium-doped barium cerate ($BaCe_{0.8}Gd_{0.2}O_{3-\delta}$ or BCG) and Zr-doped BCG under OCM operating conditions. The rationale behind studying the Zr-doped sample is that doped barium zirconates ($BaZrO_3$) are in general more resistant to CO_2 than doped barium cerates[30,32]. We present conversion-selectivity and conversion-yield curves that illustrate the OCM performance of the BCG and Zr-doped BCG powders in a packed bed reactor. The phase instability of BCG under OCM conditions is confirmed and related to the presence of CO_2, with higher CO_2 concentrations leading to more rapid transformation of BCG into $BaCO_3$, CeO_2 and Gd_2O_3 like phases. We show that the phase stability of BCG in OCM can be improved by doping with Zr without significantly affecting the C_2 yields obtained. To our knowledge, the phase structure and performance stability of gadolinium-doped barium cerate powders in OCM has not been previously investigated.

2. Experimental

2.1. Catalyst synthesis

The doped barium cerate powders were synthesized using a modified pechini method described partly elsewhere [34]. In this method, ethylenediaminetetraacetic acid (EDTA, Fisher Scientific, 99.7%) was mixed with deionized water followed by the addition of aqueous ammonia (29% NH_4OH, Fisher Scientific) to aid the dissolution of EDTA and adjust the pH of the solution to ~10. In another flask, barium nitrate (Sigma Aldrich, ≥99%) was dissolved in deionized water. The EDTA/NH_4OH solution was added to the barium nitrate solution under continuous stirring at 353 K (solution A). In a third flask, stoichiometric amounts of cerium (III) nitrate hexahydrate (Acros Organics, 99.5%) and gadolinium (III) nitrate hexahydrate (Acros Organics, 99.9%) required to form the composition of BCG were dissolved in deionized water (solution B). For the $BaCe_{0.4}Zr_{0.4}Gd_{0.2}O_{3-\delta}$ (BCZG) catalyst, a stoichiometric amount of zirconium dinitrate oxide hydrate (Alfa Aesar, 99.9%) was also added to solution B. Solution B was added dropwise to solution A while stirring at 353 K. Subsequently, ethylene glycol (J.T. Baker) was added to the mixture. The EDTA/metal ion and EDTA/ethylene glycol molar ratio used in synthesis were 1.5 and 1/3, respectively. The resulting mixture was sealed and left to stir overnight at 353 K to promote polymerization, and then evaporated at the same temperature until a viscous gel was formed. The gel was calcined at 523 K for 2 h with temperature ramps of 2 K/min resulting in a black ash. The ash was lightly grinded using a mortar and pestle then calcined again at 1273 K for 4 h with temperature ramps of 2 K/min to form the final powder.

2.2. Catalyst characterization

The X-ray Diffraction (XRD) patterns of the catalyst powders was obtained using a Rigaku MiniFlex 600 spectrometer (Cu Kα source, λ = 1.54059 Å) equipped with JADE software for phase identification and data processing. The device was operated at a tube voltage and current of 40 kV and 15 mA, respectively. A continuous sweep mode was used to collect the data in a 2Θ range from 20 to 90 at a speed of 2°(2Θ) per minute and a step size of 0.02°. The BET surface areas of the catalysts were measured using a Micrometrics 3-Flex Surface Characterization Analyzer. Prior to the BET measurement, the catalysts were degassed under vacuum at 698 K for 4 h to remove moisture and other adsorbed volatiles. Bulk composition of the materials was measured using Wavelength Dispersive X-ray Spectrometry (WDS), using a Cameca SX100 electron probe microanalyzer (EPMA) at the University of Michigan Electron Microbeam Analysis Lab (EMAL). WDS measurements were conducted using a focused electron beam with an accelerating voltage of 15 keV and a beam current of 20 nA. Synthetic zircon (Zr Lα), synthetic gadolinium-aluminum garnet (Gd Lα), synthetic alforsite (Ba Lα) and synthetic $CePO_4$ (Ce Lα) were used for calibration. Compositions were calculated from raw intensities using the X-PHI intensity correction method [35]. In preparation for WDS measurements, the catalyst powders were pressed into cylindrical pellets, sintered at 1650 °C to reduce porosity and polished to reduce surface defects.

2.3. OCM catalytic tests

Prior to the catalyst tests, the synthesized powders were pressed, crushed and sifted to agglomerates of ~125–350 μm in diameter.

Unless stated otherwise, approximately 110 mg of sifted powder was used in each experiment. The sifted powder was positioned in the center of a 6.35 mm ID quartz tube and held in place with silica wool on both sides. The quartz tube containing the catalyst powder was oriented horizontally in a furnace and heated to the desired temperature at a rate of 2 K/min under argon flow. A thermocouple was positioned next to the center of the quartz tube to monitor the reactor temperature. At the desired reactor temperature, methane (containing 5% helium) and air were fed to the reactor through mass flow controllers (Cole-Palmer) and the argon flow was discontinued. The effluent gases leaving the reactor were analyzed in a Varian CP-3800 gas chromatograph (GC) equipped with thermal conductivity and flame ionization detectors. The GC was calibrated for each measured component using certified gas mixtures supplied by Cryogenic Gases (PurityPlus). The methane conversion, C_{2+} selectivity and C_{2+} yield were calculated using equations reported in our previous work [26], where C_{2+} denotes ethane, ethylene, propane and propylene. In all experiments, the estimated carbon balance was ≥96%. The data points reported are averages of at least 3 experimental measurements and the error bars represent the calculated standard deviations.

3. Results and discussion

3.1. Synthesis

The XRD spectra of the as-synthesized BCG and BCZG powders are shown in Fig. 1. The spectra confirm that the perovskite structures were successfully obtained without the presence of significant secondary phases. The spectra also show that the peak positions from BCZG is at slightly higher angles compared to BCG which is expected as the perovskite unit volume should decrease when the Zr^{4+} ion of smaller ionic radius (R^{IV} = 0.72 Å) partially replaces the larger Ce^{4+} ion (R^{IV} = 0.87 Å) [32,36]. The estimated BET surface area of the as-synthesized BCG and BCZG catalyst were ~3.7 m^2/g and 6.5 m^2/g, respectively. Such low surface area is expected for unsupported perovskite oxide catalysts calcined in air at a high temperature of 1273 K [37,38]. Table 1 shows the bulk composition of the BCG and BCZG catalysts from stoichiometric calculations and WDS measurements. The stoichiometric weight (%) was calculated based on the weight of each metal element required for the synthesis of the catalysts. As shown in Table 1, the WDS composition are reasonably close to the stoichiometric composition.

3.2. Catalytic performance of BCG in OCM

The data in Fig. 2 show the C_{2+} selectivity, C_{2+} yield, and methane conversion for the BCG catalyst as a function of the CH_4/O_2 feed ratio. These experiments were performed at 1023 K and the different CH_4/O_2 ratios were obtained by varying the flowrate of the methane and air streams while keeping the total flow rate constant at 100 cm^3/min. The methane stream (containing 5% He) flowrate was varied between 25–95 cm^3/min, while the air flowrate was varied between 5–75 cm^3/min. The data show that the C_{2+} selectivity decreases with increasing methane conversion which is typical for OCM catalytic reactions and attributable to increased sequential reactions of the desired C_2 products to more thermodynamically favored CO_x products at higher methane conversions. A maximum C_{2+} selectivity of ~90% was attained at a high CH_4/O_2 ratio of 86, which resulted in relatively low methane conversion. The C_{2+} yield increased with methane conversion to a maximum value of ~14% at a CH_4/O_2 ratio of 2.4. It should be noted that, at 1023 K and a CH_4/O_2 ratio of 2.4, the CH_4 conversion and C_{2+} yield obtained from experiments with silica wool only was 2.2% and 1.2%, respectively. Furthermore, at a CH_4/O_2 of 86, a methane conversion of ~0.01% was achieved in the presence of silica wool only at 1023 K. These values are considered negligible compared to that obtained in the presence of the BCG catalyst.

The BCG catalyst was tested at different temperatures while using a constant methane stream flow of 35 cm^3/min and an air flow of 65 cm^3/min (i.e., CH_4/O_2 feed ratio of 2.4). The amount of higher hydrocarbons (i.e. propane and propylene) produced in these experiments were below 0.08 mol % and considered negligible. The data in Fig. 3a show the methane conversion, C_{2+} selectivity and the C_2H_4/C_2H_6 ratio at temperatures between 1023 K and 1123 K. The data show that methane conversion was not significantly affected by temperature in the

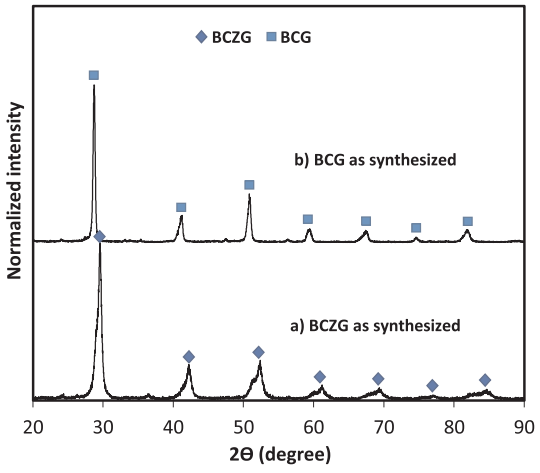

Fig. 1. XRD patterns of as-synthesized powders (a) BCZG and (b) BCG.

Table 1
Catalyst composition from stoichiometric calculations and WDS measurements.

	$BaCe_{0.8}Gd_{0.2}O_{3-\delta}$		$BaCe_{0.4}Zr_{0.4}Gd_{0.2}O_{3-\delta}$	
Element	Stoichiometric (wt. %)	WDS (wt. %)	Stoichiometric (wt. %)	WDS (wt. %)
Ba	41.8	39.6	44.4	42.6
Ce	34.1	35.3	18.1	19.9
Zr	–	–	11.8	10.4
Gd	9.6	9.4	10.2	8.7

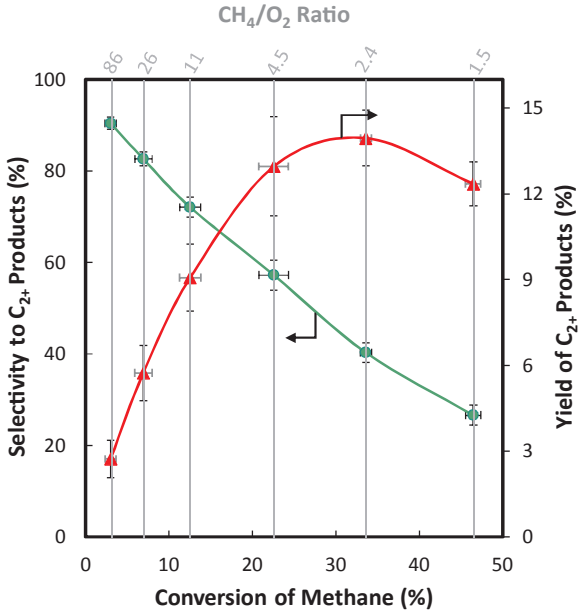

Fig. 2. Dependence of C_{2+} selectivity, C_{2+} yield and methane conversion from BCG catalyst on CH_4/O_2 feed ratio. Temperature = 1023 K. Total flow = 100 cm^3/min. Catalyst weight = 110 mg.

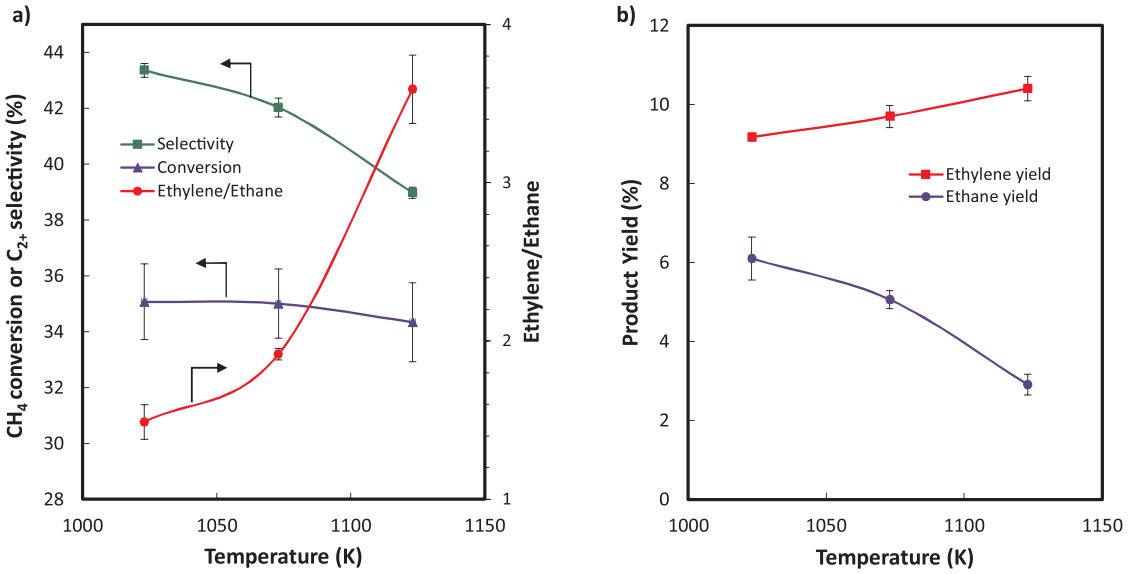

Fig. 3. Effect of temperature on (a) CH_4 conversion, C_{2+} selectivity and C_2H_4/C_2H_6 ratio, (b) Ethylene and Ethane yields, from BCG catalyst. Total flow = 100 cm^3/min. CH_4/O_2 = 2.4. Catalyst weight = 110 mg.

studied temperature range which is expected since oxygen is nearly exhausted (oxygen conversion ≥97%) at these conditions. The effect of temperature on methane conversion is expected to become significant under conditions where the oxygen conversion is relatively low (e.g., lower temperatures). The data also show that the overall C_{2+} selectivity decreases while the C_2H_4/C_2H_6 ratio increases with increasing temperature. This is accompanied by a decrease in the yield of ethane, and an increase in the yield of ethylene as shown in Fig. 3b. The data indicates increased occurrence of sequential reactions of ethane to ethylene and CO_x at higher temperatures.

3.3. Stability studies of BCG in OCM

The spent catalyst was collected and characterized using XRD. The XRD spectrum of the spent BCG catalyst is shown in Fig. 4b. This catalyst was characterized after testing for several hours at 1023 K, using CH_4/O_2 ratios ranging from 1.5 to 86 consecutively. The spectrum of unreacted BCG catalyst is also included (Fig. 4a) for comparison. Analysis of the spectrum of the reacted catalyst reveals that the BCG perovskite phase, which is required for ion and electron conduction [33], had been significantly transformed. The spectrum suggests the emergence of $BaCO_3$, CeO_2 and Gd_2O_3 like phases. This phase transformation is likely caused by a reaction of BCG with CO_2 as discussed previously.

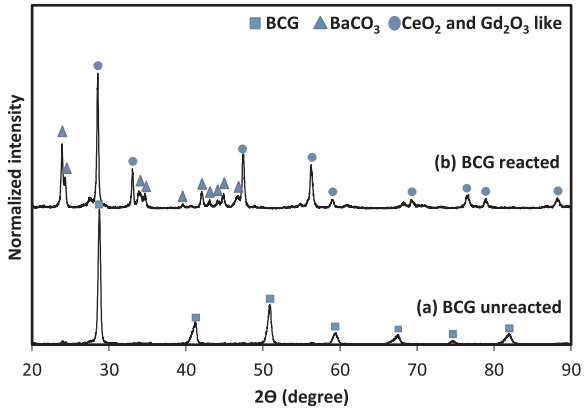

Fig. 4. XRD patterns of (a) unreacted BCG and (b) BCG reacted at 1023 K using CH_4/O_2 ratios ranging from 1.5 to 86 consecutively.

To determine the effect of CO_2 concentration on BCG phase stability in OCM, additional experiments were conducted using high and low CH_4/O_2 ratios. As shown above, the CO_2 concentration is higher at lower CH_4/O_2 ratios. These experiments were performed at 1023 K with a total flowrate of 100 cm^3/min using 200 mg of catalyst powder. In each experiment, the catalyst was heated and cooled in argon flow to minimize any chemical transformations that could occur during heating and cooling. The XRD data for the unreacted BCG catalyst and BCG catalysts reacted at different CH_4/O_2 ratios are presented in Fig. 5. The data show that the catalysts tested at a high CH_4/O_2 ratio of 26 for one hour (Fig. 5b) and six hours (Fig. 5c) largely retained their perovskite structure. On the other hand, the catalyst used for only 1 h, at a low CH_4/O_2 ratio of 2.4 (Fig. 5d), changed significantly, segregating into the $BaCO_3$, CeO_2 and Gd_2O_3 phases. The estimated CO_2 concentration at the reactor outlet was ~0.7 mol% for the reaction performed at a CH_4/O_2 ratio of 26, while it was ~6.2 mol% at a CH_4/O_2 ratio of 2.4. These data show that the phase structure of BCG is more readily decomposed at higher CO_2 concentrations. Furthermore, despite the observed changes in phase structure of the BCG catalyst, the data in Fig. 6 show that the methane conversion, C_{2+} selectivity and C_{2+} yield obtained was relatively stable over 48 h on stream using a low CH_4/O_2 ratio of 2.4. The data suggest that the phase change in the catalyst does not result in a significant change in the catalyst performance. The performance of BCG remains stable even with significant phase changes probably because at least one of the new phases formed is also active for OCM. For example, $BaCO_3$ and Ba/CeO_2 have been shown to be active for OCM in previous studies [27,28,39].

3.4. Effect of Zr doping on BCG performance and phase stability

Based on our analysis of the performance of the BCG catalyst, we conclude that this material can perform OCM with high selectivity to C_{2+} products under low O_2/CH_4 ratios. This high performance along with the ion/electron conducting properties of BCG makes it a promising material for use as membrane or catalyst in solid oxide membrane reactors for OCM. The issue with this material is that, as we described above, even small amounts of CO_2, which is inevitable at elevated (and realistic) methane conversion, results in changes in its perovskite structure. While these changes do not have much effect on the catalytic performance of this material, these changes are expected to have a dramatic effect on its ion/electron conducting properties. To address this problem of instability of the perovskite phase of BCG in

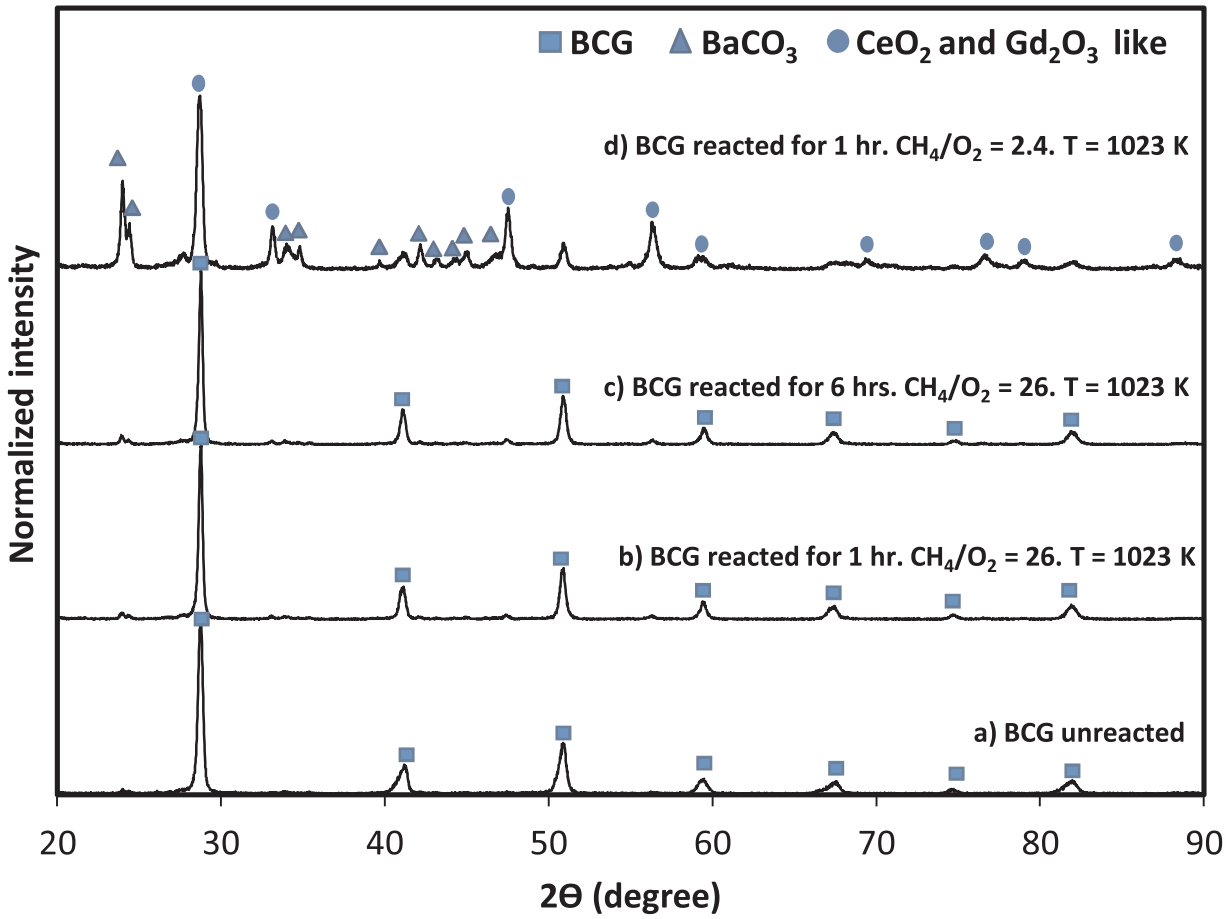

Fig. 5. XRD patterns from (a) unreacted BCG (b) BCG reacted for 1 h at CH_4/O_2 = 26 and T = 1023 K (c) BCG reacted for 6 h at CH_4/O_2 = 26 and T = 1023 K and (d) BCG reacted for 1 h at CH_4/O_2 = 2.4 and T = 1023 K.

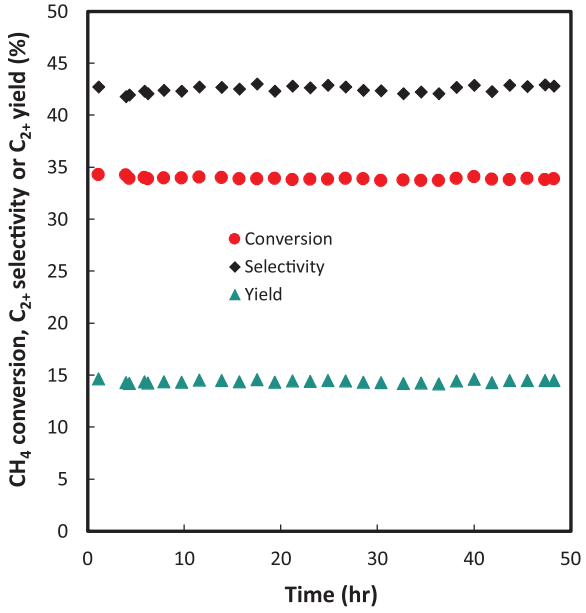

Fig. 6. Plot of CH_4 Conversion, C_{2+} selectivity and C_{2+} yield over time from BCG catalyst. Catalyst weight = 110 mg. CH_4/O_2 = 2.4. Total flow rate = 100 cm^3/min. Temperature = 1023 K.

OCM, we probed the impact of introducing Zr into the structure of BCG. As mentioned previously, the phase structure of $BaZrO_3$ is more stable than $BaCeO_3$ in CO_2 containing environment.

Data in Fig. 7a and b show respective conversion-selectivity and conversion-yield curves from the Zr-doped BCG catalyst (BCZG) and undoped BCG. These experiments were also performed at 1023 K, CH_4/O_2 ratios of 1.5–86 and using 110 mg of catalyst. The data show that the catalysts exhibit very similar performance, and that the introduction of Zr has no negative effect on the catalytic performance of BCG. Data in Fig. 8a and b show the selectivity of carbon-containing products formed during the reaction with BCG and BCZG catalyst, respectively, as a function of the methane conversion. As shown in the figures, the product distribution obtained from the BCG and BCZG catalyst is similar, which indicates a similar reaction mechanism on the both catalysts. The ethane selectivity is high at low methane conversions, which corresponds to high CH_4/O_2 ratios. As the methane conversion increases due to decreasing the CH_4/O_2 ratio, the ethane selectivity decreases monotonously. The ethylene and C_3 (propane and propylene) selectivity increase with increasing methane conversion, reach a maximum, and then decrease. The CO_x selectivity increased monotonously with increasing methane conversion (i.e., decreasing CH_4/O_2 ratio). This data indicate that ethane is the primary product formed in the reaction. The decrease in ethane selectivity and increase in CO_x selectivity with increasing methane conversion is consistent with the occurrence of higher sequential reactions of ethane to CO_x at lower CH_4/O_2 feed ratios.

The XRD spectra for unreacted and reacted BCG and BCZG catalysts are shown in Fig. 9. The spectra of the reacted catalysts were obtained from samples tested at 1023 K, a low CH_4/O_2 feed ratio of 2.4 and a total flow rate of 100 cm^3/min. The data show that there was no significant change in the phase structure of the BCZG catalyst reacted for 1 h (Fig. 9c) compared to the unreacted BCZG catalyst (Fig. 9a). New phases corresponding to $BaCO_3$, CeO_2 and Gd_2O_3 start appearing in the

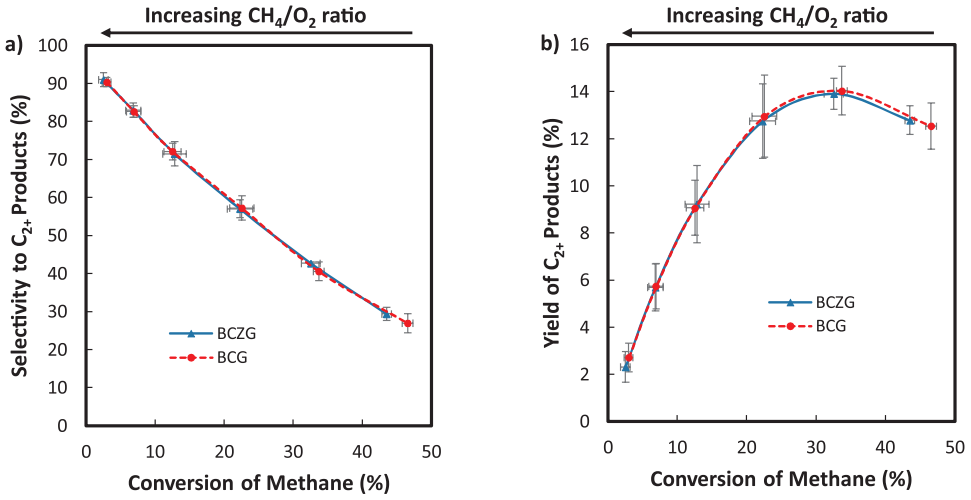

Fig. 7. (a) Conversion-selectivity curve and (b) conversion-yield curve from BCG and BCZG catalyst. Temperature = 1023 K. Total flow = 100 cm^3/min. Catalyst weight = 110 mg. CH_4/O_2 ratio = 1.5–86. The CH_4/O_2 ratio increases from the right to the left of the plots as indicated by the arrows above the figures.

BCZG catalyst reacted for over 48 h (Fig. 9d). Comparison between the XRD spectrum of the BCG catalyst reacted for 1 h (Fig. 9e) and the spectra of the reacted BCZG catalysts showed that the introduction of Zr to BCG improves phase stability, without changing the C_{2+} yields. Fig. 10 presents a plot of CH_4 conversion, C_{2+} selectivity and C_{2+} yield from BCZG over time using a CH_4/O_2 ratio of 2.4. The data show that the catalytic performance was relatively stable over 48 h.

4. Conclusions

We performed OCM tests on $BaCe_{0.8}Gd_{0.2}O_{3-\delta}$ (BCG) powders in a packed bed reactor and obtained high C_{2+} selectivities (up to 90%) at low O_2 partial pressures expected to occur in membrane reactors. For the conditions tested, a maximum C_{2+} yield of ~14% was achieved at 1023 K and a CH_4/O_2 feed ratio of 2.4. Under this reaction condition, phase segregation of BCG into $BaCO_3$, CeO_2 and Gd_2O_3 like phases occurred, and this phase instability was related to the presence of CO_2. While this phase transformation is not detrimental to the CH_4 conversion, C_{2+} selectivity and C_{2+} yield, the loss of the perovskite structure is detrimental to the ionic and electronic conductivity of the material, which is important for its application in OCM membrane reactors. We showed that by doping BCG with Zr, the phase instability in OCM is suppressed without significantly affecting the C_2 yields.

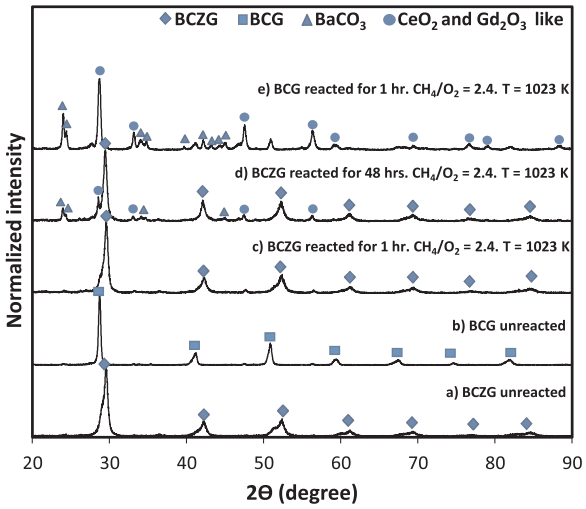

Fig. 9. XRD patterns of (a) unreacted BCZG (b) unreacted BCG (c) BCZG reacted for 1 h at CH_4/O_2 = 2.4 and T = 1023 K (d) BCZG reacted for 48 h at CH_4/O_2 = 2.4 and T = 1023 K (e) BCG reacted for 1 h at CH_4/O_2 = 2.4 and T = 1023 K.

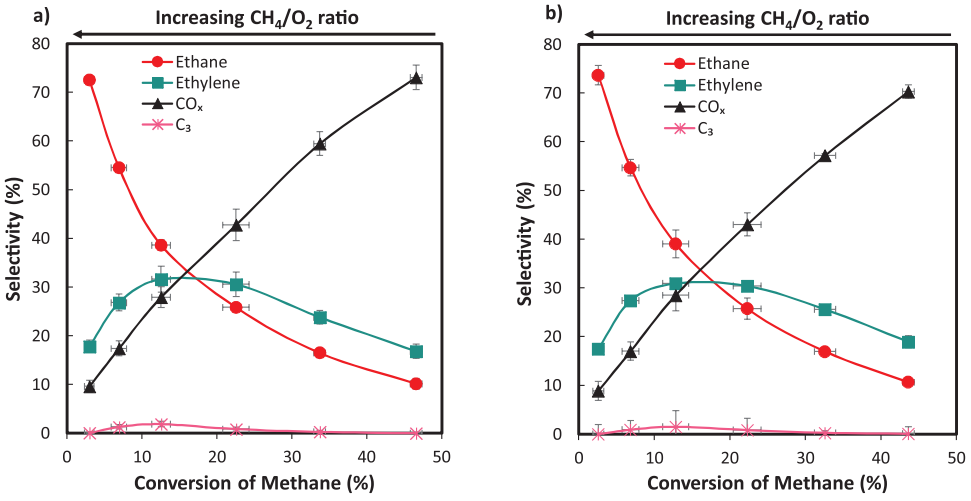

Fig. 8. Selectivity of carbon-containing products (C_2H_6, C_2H_4, CO_x and C_3) as a function of methane conversion for (a) BCG catalyst (b) BCZG catalyst. C_3 represents propane and propylene. The CH_4/O_2 ratio increases from the right to the left of the plots as indicated by the arrows above the figures.

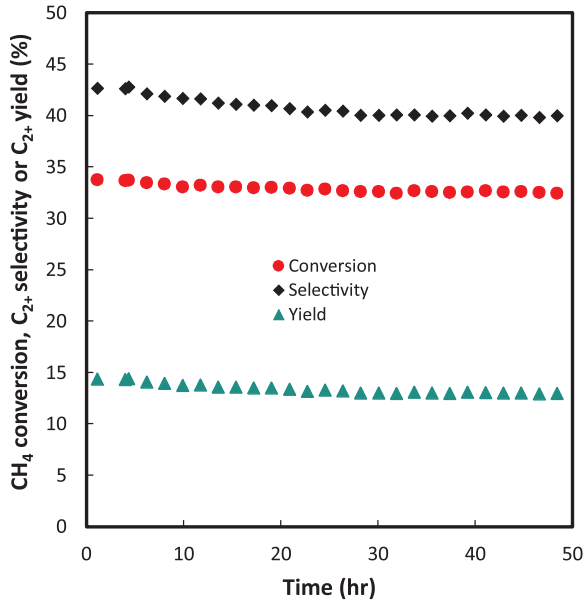

Fig. 10. Plot of CH_4 Conversion, C_{2+} selectivity and C_{2+} yield over time from BCZG catalyst. Catalyst weight = 110 mg. CH_4/O_2 = 2.4. Total flow rate = 100 cm^3/min. Temperature = 1023 K.

Acknowledgements

This work was primarily supported by the U.S. Department of Energy, Office of Basic Energy Science, Division of Chemical Sciences (FG-02- 05ER15686). The authors acknowledge financial support from ExxonMobil Research and Engineering. V.O.I. acknowledges support from the Nigerian Government under the Presidential Special Scholarship Scheme for Innovation and Development (PRESSID).

References

[1] U.S. Crude Oil, Natural Gas, and Natural Gas Proved Reserves, Year-end 2015, (n.d.). http://www.eia.gov/naturalgas/crudeoilreserves/ (Accessed January 16, 2017).
[2] R. Horn, R. Schlögl, Methane activation by heterogeneous catalysis, Catal. Lett. 145 (2014) 23–39, http://dx.doi.org/10.1007/s10562-014-1417-z.
[3] E. McFarland, Unconventional chemistry for unconventional natural gas, Science 338 (2012) 340–342.
[4] X. Guo, G. Fang, G. Li, H. Ma, H. Fan, L. Yu, C. Ma, X. Wu, D. Deng, M. Wei, et al., Direct, nonoxidative conversion of methane to ethylene, aromatics, and hydrogen, Science 344 (2014) 616–619.
[5] A.I. Olivos-Suarez, À. Szécsényi, E.J. Hensen, J. Ruiz-Martinez, E.A. Pidko, J. Gascon, Strategies for the direct catalytic valorization of methane using heterogeneous catalysis: challenges and opportunities, ACS Catal. 6 (2016) 2965–2981.
[6] P. Schwach, X. Pan, X. Bao, Direct conversion of methane to value-added chemicals over heterogeneous catalysts: challenges and prospects, Chem. Rev. 117 (2017) 8497–8520, http://dx.doi.org/10.1021/acs.chemrev.6b00715.
[7] E.V. Kondratenko, T. Peppel, D. Seeburg, V.A. Kondratenko, N. Kalevaru, A. Martin, S. Wohlrab, Methane conversion into different hydrocarbons or oxygenates: current status and future perspectives in catalyst development and reactor operation, Catal. Sci. Technol. 7 (2017) 366–381, http://dx.doi.org/10.1039/C6CY01879C.
[8] G.E. Keller, M.M. Bhasin, Synthesis of ethylene via oxidative coupling of methane: I. Determination of active catalysts, J. Catal. 73 (1982) 9–19.
[9] U. Zavyalova, M. Holena, R. Schlögl, M. Baerns, Statistical analysis of past catalytic data on oxidative methane coupling for new insights into the composition of high-performance catalysts, ChemCatChem. 3 (2011) 1935–1947, http://dx.doi.org/10.1002/cctc.201100186.
[10] D.J. Driscoll, W. Martir, J.X. Wang, J.H. Lunsford, Formation of gas-phase methyl radicals over magnesium oxide, J. Am. Chem. Soc. 107 (1985) 58–63.
[11] L. Luo, X. Tang, W. Wang, Y. Wang, S. Sun, F. Qi, W. Huang, Methyl radicals in oxidative coupling of methane directly confirmed by synchrotron VUV photoionization mass spectroscopy, Sci. Rep. 3 (2013) 1625, http://dx.doi.org/10.1038/srep01625.
[12] Z. Stansch, L. Mleczko, M. Baerns, Comprehensive kinetics of oxidative coupling of methane over the La2O3/CaO catalyst, Ind. Eng. Chem. Res. 36 (1997) 2568–2579.
[13] S. Arndt, T. Otremba, U. Simon, M. Yildiz, H. Schubert, R. Schomäcker, Mn–Na 2 WO 4/SiO 2 as catalyst for the oxidative coupling of methane. What is really known? Appl. Catal. Gen. 425 (2012) 53–61.
[14] S. Arndt, G. Laugel, S. Levchenko, R. Horn, M. Baerns, M. Scheffler, R. Schlögl, R. Schomäcker, A critical assessment of Li/MgO-based catalysts for the oxidative coupling of methane, Catal. Rev. 53 (2011) 424–514, http://dx.doi.org/10.1080/01614940.2011.613330.
[15] B.L. Farrell, V.O. Igenegbai, S. Linic, A viewpoint on direct methane conversion to ethane and ethylene using oxidative coupling on solid catalysts, ACS Catal. 6 (2016) 4340–4346, http://dx.doi.org/10.1021/acscatal.6b01087.
[16] J.C.W. Kuo, C.T. Kresge, R.E. Palermo, Evaluation of direct methane conversion to higher hydrocarbons and oxygenates, Catal. Today 4 (1989) 463–470, http://dx.doi.org/10.1016/0920-5861(89)85042-4.
[17] Ja. Labinger, K.C. Ott, Mechanistic studies on the oxidative coupling of methane, J. Phys. Chem. 91 (1987) 2682–2684, http://dx.doi.org/10.1021/j100295a003.
[18] T.P. Tiemersma, M.J. Tuinier, F. Gallucci, J.A.M. Kuipers, M. van Sint Annaland, A kinetics study for the oxidative coupling of methane on a Mn/Na 2 WO 4/SiO 2 catalyst, Appl. Catal. Gen. 433 (2012) 96–108.
[19] X. Tan, Z. Pang, Z. Gu, S. Liu, Catalytic perovskite hollow fibre membrane reactors for methane oxidative coupling, J. Membr. Sci. 302 (2007) 109–114, http://dx.doi.org/10.1016/j.memsci.2007.06.033.
[20] X. Tan, K. Li, Oxidative coupling of methane in a perovskite hollow-fiber membrane reactor, Ind. Eng. Chem. Res. 45 (2006) 142–149, http://dx.doi.org/10.1016/0926-860X(95)00098-4.
[21] Y. Lu, A.G. Dixon, W.R. Moser, Y.H. Ma, U. Balachandran, Oxygen-permeable dense membrane reactor for the oxidative coupling of methane, J. Membr. Sci. 170 (2000) 27–34, http://dx.doi.org/10.1016/S0376-7388(99)00354-3.
[22] N.H. Othman, Z. Wu, K. Li, A micro-structured La 0.6 Sr 0.4 Co 0.2 Fe 0.8 O 3- δ hollow fibre membrane reactor for oxidative coupling of methane, J. Membr. Sci. 468 (2014) 31–41.
[23] F.T. Akin, Y.S. Lin, Oxidative coupling of methane in dense ceramic membrane reactor with high yields, AIChE J. 48 (2002) 2298–2306, http://dx.doi.org/10.1002/aic.690481019.
[24] B. Wang, S. Albarracín-Suazo, Y. Pagán-Torres, E. Nikolla, Advances in methane conversion processes, Catal. Today (2017) 1–12, http://dx.doi.org/10.1016/j.cattod.2017.01.023.
[25] J. Sunarso, S. Baumann, J.M. Serra, W.A. Meulenberg, S. Liu, Y.S. Lin, J.D. Da Costa, Mixed ionic–electronic conducting (MIEC) ceramic-based membranes for oxygen separation, J. Membr. Sci. 320 (2008) 13–41.
[26] B. Farrell, S. Linic, Oxidative coupling of methane over mixed oxide catalysts designed for solid oxide membrane reactors, Catal. Sci. Technol. 6 (2016) 4370–4376.
[27] C.T. Au, K.D. Chen, C.F. Ng, The modification of Gd 2 O 3 with BaO for the oxidative coupling of methane reactions, Appl. Catal. Gen. 170 (1998) 81–92.
[28] K. Otsuka, Y. Shimizu, T. Komatsu, Ba doped cerium oxides active for oxidative coupling of methane, Chem. Lett. 16 (1987) 1835–1838.
[29] T. Hibino, T. Sato, K. Ushiki, Y. Kuwahara, Membrane reactor for oxidative coupling of CH4 with an oxide ion–electron hole mixed conductor, J. Chem. Soc. Faraday Trans. 91 (1995) 4419–4422.
[30] D.A. Medvedev, J.G. Lyagaeva, E.V. Gorbova, A.K. Demin, P. Tsiakaras, Advanced materials for SOFC application: strategies for the development of highly conductive and stable solid oxide proton electrolytes, Prog. Mater. Sci. 75 (2016) 38–79, http://dx.doi.org/10.1016/j.pmatsci.2015.08.001.
[31] M. Talimi, V. Thangadurai, Electrical conductivity and chemical stability of perovskite-type BaCe0.8-x Ti x Y0.2O3-δ, Ionics 17 (2011) 195–200, http://dx.doi.org/10.1007/s11581-011-0522-x.
[32] K.H. Ryu, S.M. Haile, Chemical stability and proton conductivity of doped BaCeO 3–BaZrO 3 solid solutions, Solid State Ion. 125 (1999) 355–367.
[33] Y. Wang, H. Wang, T. Liu, F. Chen, C. Xia, Improving the chemical stability of BaCe 0.8 Sm 0.2 O 3- δ electrolyte by Cl doping for proton-conducting solid oxide fuel cell, Electrochem. Commun. 28 (2013) 87–90.
[34] V. Agarwal, M. Liu, Preparation of barium cerate-based thin films using a modified Pechini process, J. Mater. Sci. 32 (1997) 619–625.
[35] C. Merlet, An accurate computer correction program for quantitative electron probe microanalysis, Microchim. Acta 114 (1994) 363–376.
[36] C. Zuo, S.E. Dorris, U. Balachandran, M. Liu, Effect of Zr-doping on the chemical stability and hydrogen permeation of the Ni-BaCe0. 8Y0. 2O3-α mixed protonic-electronic conductor, Chem. Mater. 18 (2006) 4647–4650.
[37] J. Kirchnerova, D. Klvana, J. Vaillancourt, J. Chaouki, Evaluation of some cobalt and nickel based perovskites prepared by freeze-drying as combustion catalysts, Catal. Lett. 21 (1993) 77–87.
[38] N. Gunasekaran, S. Saddawi, J.J. Carberry, Effect of surface area on the oxidation of methane over SolidOxide solution catalyst La 0.8 Sr 0.2 MnO 3, J. Catal. 159 (1996) 107–111.
[39] K. Aika, T. Moriyama, N. Takasaki, E. Iwamatsu, Oxidative dimerization of methane over BaCO 3, SrCO 3 and these catalysts promoted with alkali, J. Chem. Soc. Chem. Commun. (1986) 1210–1211.